DOI: 10.1002/ejic.200700364

3D Architectures of InOOH: Ultrasonic-Assisted Synthesis, Growth Mechanism, and Optical Properties

Liyong Chen,[a] Xuchu Ma,[a] Yankuan Liu,[a] Yan'ge Zhang,[a] Weizhi Wang,[a] Yi Liang,[a] and Zude Zhang*[a]

Keywords: Indium / Mechanism / UV/Vis spectroscopy / Solvothermal synthesis

An ultrasonic-assisted solvothermal route based on the hydrolysis of In^{3+} was utilized to synthesize InOOH with a hierarchic three-dimensional (3D) architecture, which was assembled by single-crystalline nanowires with diameters of about 10 nm and lengths up to several hundred nanometers. X-ray powder diffraction (XRD), field emission scanning electron microscopy (FE-SEM), transmission electron microscopy (TEM), and FTIR spectra were used to characterize the obtained products. Alkaline media and solvent play crucial roles in influencing the phase and the morphology of the products. A possible mechanism was proposed to explain the formation process of the InOOH 3D nanostructure. The optical properties of InOOH was also investigated by ultraviolet and visible (UV/Vis) spectroscopy, which indicated that InOOH is a wide band-gap semiconductor.

Introduction

In the past few years the synthesis of materials has essentially focused on size and shape and dimensionality control.[1] To date, challenges in the synthesis of nanomaterials include the control of morphology and the assemblage of ensembles of nanostructures. Because hierarchical structures may provide new forms with extremely high surface-to-volume ratios with potential applications as new catalysts or as a scaffolding support, nanoscale units used to build complex and hierarchical nanoarchitectures have attracted significant interest in material synthesis and device fabrication; some of these architectures include hierarchical three-dimensional (3D) MnS[2] and TiO_2,[3] flower-like iron oxide[4] and AlOOH,[5] dandelion-like CuO[6] and ZnO,[7] and urchin-like NiS[8] and WO_3.[9] Previously, several synthetic strategies were developed to fabricate 3D architectures assembled from nanowires, where polymers or solid templates were required to control the highly oriented growth of the nanowires.[10] However, the use of additives (i.e. polymers, templates) would increase the production cost and also introduce heterogeneous impurities. Thus, it is still a significant project to develop facile, additive-free, and easily controlled synthetic methods for the construction of 3D architectures of anisotropic materials.

Nanometer-scale indium oxyhydroxide (InOOH) and indium sesquioxide (In_2O_3) have found applications in the fields of semiconductors and optical materials.[11] InOOH, the hydrate of In_2O_3,[12] can be directly formed by the dehydration of $In(OH)_3$. Further calcination of InOOH at ambient pressure will produce metastable corundrum-type In_2O_3, an important n-type semiconductor with a direct bandgap of ca. 3.6 eV.[11b,13] To the best of our knowledge, many efforts have been made to synthesize micro- and/or nanostructured InOOH with different morphologies, such as nanofibers,[13a] nanotubes,[13b] and hollow spheres.[11c] However, hierarchical InOOH architectures consisting of nanoscale units have seldom been reported. Recently, sonochemical methods were proposed to synthesize nanomaterials with various structures,[14] because ultrasonic sound waves can provide energy by radiating through a solution and causing alternative high and low pressures in the liquid medium. The energy released from sonication can lead to enhanced chemical reactivity and accelerated reaction rates. Herein, we address our recent work on the synthesis of hierarchically 3D InOOH architectures composed of uniform nanowires, which involves an additives-free ultrasonic-assisted solvothermal route. This method uses the reaction among ethylenediamine (En), water, and In^{3+}. On the basis of investigations on the effect of En, we find that it might server as the structure-directing agent in the formation of InOOH nanowires, similar to the role of En as a structure-directing coordination template in previous studies.[15] Moreover, the UV/Vis spectrum showed that InOOH with a hierarchical 3D architecture is a typical wide band-gap semiconductor with E_g of ca. 4.44 eV, which suggests that InOOH has the potential to be used in optical devices.

[a] Department of Chemistry, University of Science and Technology of China,
Hefei, Anhui 230026, P. R. China
Fax: +86-551-3601592
E-mail: zzd@ustc.edu.cn

Results and Discussion

Figure 1 shows the XRD pattern of the products prepared at 210 °C for 24 h. All the diffraction peaks can be indexed to orthorhombic InOOH with cell parameters a = 5.23 Å, b = 4.55 Å, and c = 3.26 Å, which are in good agreement with values from the standard card (JCPDS No. 71-2277). The XRD pattern confirms a highly crystalline nature of InOOH. Note that the diffraction peaks become broad, indicating that the size of the domain may be small.

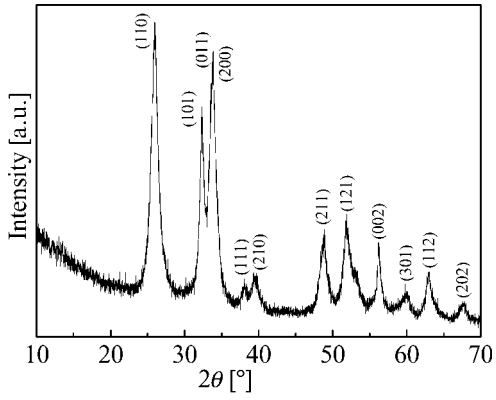

Figure 1. XRD pattern of InOOH prepared at 210 °C for 24 h.

The morphology and structure of the products obtained at 210 °C for 24 h were determined by FE-SEM and TEM. Figure 2a shows a panoramic FE-SEM image that shows that the samples have hierarchical 3D architectures with sizes in the range of several hundred nanometers to 1 μm. Figure 2b is a high-magnification FE-SEM image and Figures 2c–e are TEM images. Through careful observation (Figure 2b, d), we find that the architectures consist of nanowires with uniform diameters of ca. 10 nm and lengths up to several hundred nanometers. The nanowires were also investigated by the selected area electron diffraction (SAED) pattern and high-resolution transmission electron microscopy (HR-TEM). In the SAED pattern (Figure 2e, inset), the first diffraction ring corresponds to the (110) plane reflection of the orthorhombic InOOH structure. Owing to the fact that the atomic plane spacings of (101), (011), and (200) are very close, and that these three reflection rings look like one, the second diffraction ring cannot be distinguished well. Figure 2f is a HRTEM image, taken from a randomly chosen nanowire, where the average value of the plane spacing along the vertical direction is ca. 0.265 nm, and the value of the plane spacing along the inclined direction is about 0.279 nm. These two series of interplanar spacings correspond to the d spacing of the (101) and (200) planes of orthorhombic InOOH, respectively. These results further confirm the single-crystal nature of the samples.

In this strategy, we explored the influencing factors and optimized the reaction conditions; we coupled this with the appropriate choice of alkaline media and solvent to control the phase and the morphology of the obtained products. Sonication was extensively used for the generation of zero-

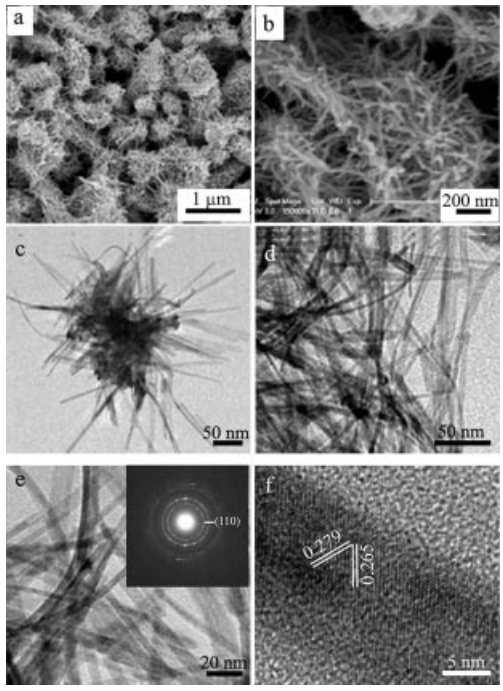

Figure 2. (a) Panoramic and (b) high-magnification FE-SEM images of InOOH with 3D architectures; (c) low-magnification TEM image of InOOH with 3D architectures; (d) high-magnification TEM image taken from their edge; (e) TEM image of InOOH nanowires (inset is SAED pattern); (f) HRTEM image of a single InOOH nanowire.

dimensional (0D) and one-dimensional (1D) nanostructures, as sonication is generally used as the driving force for nucleation. Here, we utilized the energy from the sonication process to induce the formation of uniform seeds,[14c] which favored the formation of nanowires with uniform diameters under solvothermal conditions. The TEM image (Figure 3a) reveals that the morphology of the products prepared without presonication have 3D structures composed of nonuniform nanowires. Figure 3b presents a high-magnification TEM image taken from their edge, which further testifies to the fact that the diameter of these nanowires are not uniform.

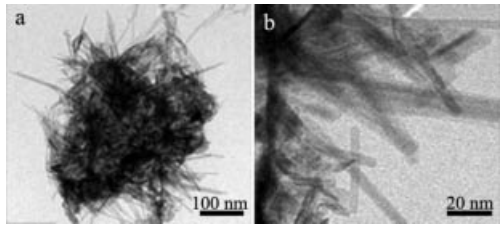

Figure 3. (a) Low-magnification TEM image of 3D InOOH architectures; (b) high-magnification TEM image recorded at the edge of the InOOH 3D architectures that shows nanowires with nonuniform diameters. These InOOH products were prepared without sonication.

As far as the alkaline media was concerned, En was found to be important in determining the phase and the morphology of the products. En acts as a structure-direct-

ing coordination agent to obtain InOOH nanowires as a result of it being a good ligand. En also provides the basicity for the system and facilitates the hydrolysis reaction of In^{3+} and the formation of the orthorhomic InOOH phase. To better understand the role of En in this synthetic process, different organic amines such as hexamethylene diamine or diethylamine were used as a substitute for En in controlled experiments. Figures 4a, b show TEM images of the products prepared in both parallel experiments; both products are solid quasispherical structures composed of nanoparticles. Their phases are characterized by XRD patterns (Figure 4c), where all diffraction peaks can be indexed to cubic In_2O_3 (JCPDS No. 76-0152). Obviously, En may play a crucial factor in determining the phase and morphology of InOOH. To further explore the function of En, the intermediate products prepared in the initial 1, 2, 6, and 24 h were studied by FTIR as shown in Figure 4d, Curves 1–4, respectively. Figure 4d, Curve 1 clearly displays peaks at 3220 and 3097 cm^{-1} for the –NH stretching vibration; it is shifted to lower wavenumbers than that of free En, whereas peaks at 2936 and 2890 cm^{-1} for the $–CH_2$ stretching vibration and the peak at 1580 cm^{-1} for the –NH bending vibration are shifted to higher wavenumbers relative to free En.[15c,16] These data confirm that the coordinative effect of En mostly exists in our experiments. Curves 3 and 4 (Figure 4d) exhibit two peaks at 3425 and 1980 cm^{-1} together with a broad band at 2700 cm^{-1} for the –OH vibration of InOOH and another peak at 445 cm^{-1} for the In–O vibration absorption,[11c,17] which reveals that InOOH has already formed after the initial 6 h. On the contrary, the intensity of the characteristic absorption peaks of En gradually decreases, whereas those of InOOH gradually increase with prolonged reaction times. These experimental results reveal that En is the optimum alkaline medium and has a great influence on the growth of InOOH with 3D architectures.

To further investigate the mechanism of formation of InOOH with a hierarchical 3D architecture, time-dependent experiments involved in growth processes were conducted. The products prepared at various stages were followed by TEM imaging. Figure 5 shows TEM images of the intermediate samples obtained at 1, 2, 6, 8, 12, and 36 h. At the initial stage there are many nanoparticles formed with small sizes (Figure 5a, b). With prolonged reaction times, some short nanorods are developed at the expense of these small nanoparticles (Figure 5c). After longer reaction times, the nanoparticles gradually disappear and nanorods slowly grow into long nanowires (Figure 5d, e). These images clearly show the transformation process of the products from nanoparticles to nanorods and then to nanowires. However, the obtained sample has a 3D architecture composed of nonuniform nanowires (Figure 5f) when the reaction time is prolonged to 36 h, which reveals that an increase in the reaction time to greater than 24 h is unfavorable for the formation of uniform nanowires. The evolution of the products was also tracked by XRD (Figure 6a–f). As shown in Figure 6a, the product formed in the initial first hour is amorphous. From Figure 6b, it is found that there

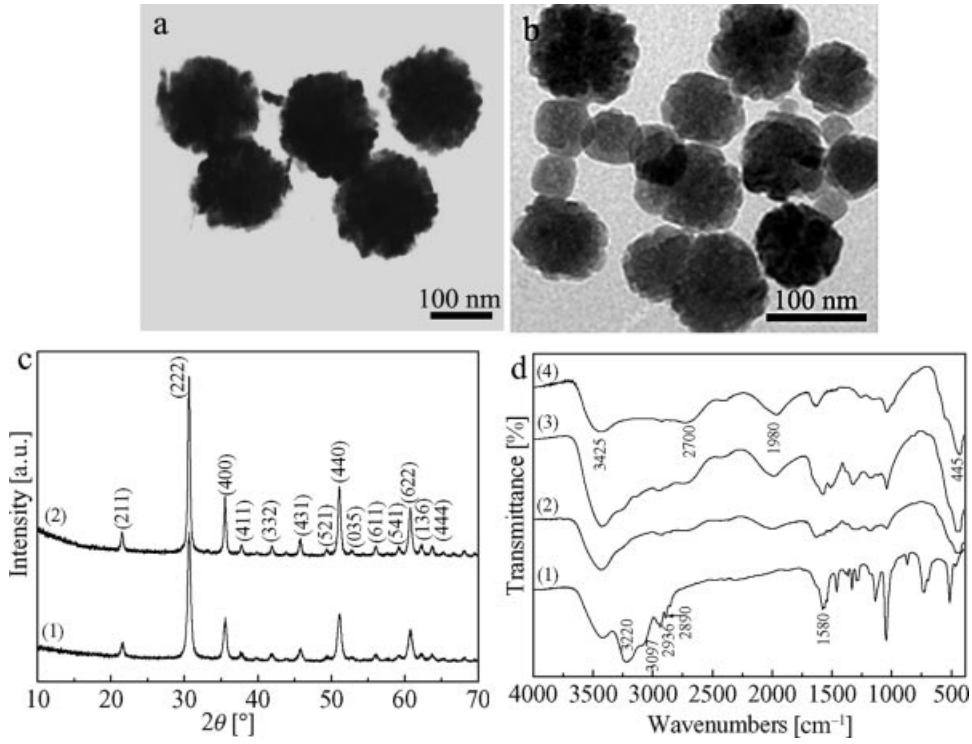

Figure 4. TEM images of samples obtained in alkaline media of (a) hexamethylene diamine; (b) diethylamine; (c) XRD patterns of samples obtained in (1) hexamethylene diamine and (2) diethylamine; (d) FTIR spectra of intermediate samples prepared in alkaline media of ethylenediamine and at 210 °C for (1) 1 h, (2) 2 h, (3) 6 h, and (4) 24 h.

is a diffraction peak at 22.4°, which corresponds to the diffraction of (200) lattice plane of cubic $In(OH)_3$ (JCPDS No. 85-1338) and indicates that the products already exist as cubic $In(OH)_3$ phases in the initial 2 h. By increasing the reaction time to 6 h and then 8 h, the diffraction peak of the (200) lattice plane increases firstly (Figure 6c), but then gradually decreases (Figure 6d). When the reaction time reaches 12 h, the diffraction peak completely disappears (Figure 6e). The orthorhombic InOOH diffraction peaks are also observed in the initial 2 h, and they progressively become sharper and stronger with longer reaction times. When the reaction time is increased to 36 h, a highly crystalline InOOH phase is obtained (Figure 6f). On the basis of these XRD patterns there is evidence to support a "dissolution–recrystallization" process. The $In(OH)_3$, nanoparticles are first formed and then slowly dissolved together with the gradual formation of InOOH nanocrystals owing to the fact that the solubility of $In(OH)_3$ is larger than that of InOOH. Hence, the phase transformation from $In(OH)_3$ to InOOH exists in this strategy, and the reactions can be simply expressed in Equations (1) and (2).

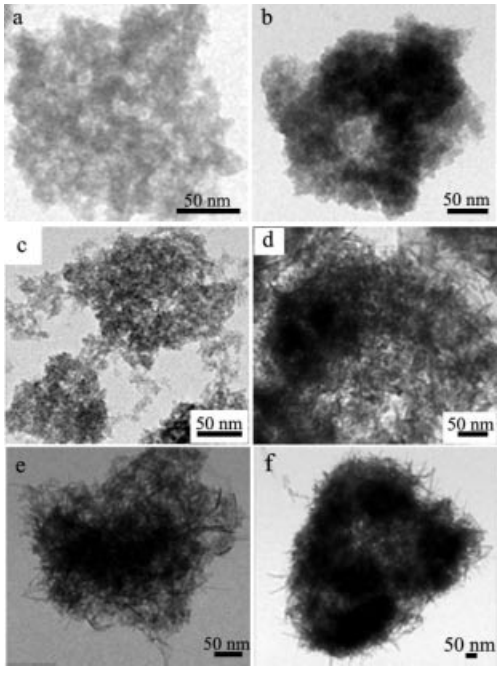

Figure 5. TEM images of intermediate products obtained in the presence of ethylenediamine and at 210 °C for (a) 1 h; (b) 2 h; (c) 6 h; (d) 8 h; (e) 12 h; and (f) 36 h.

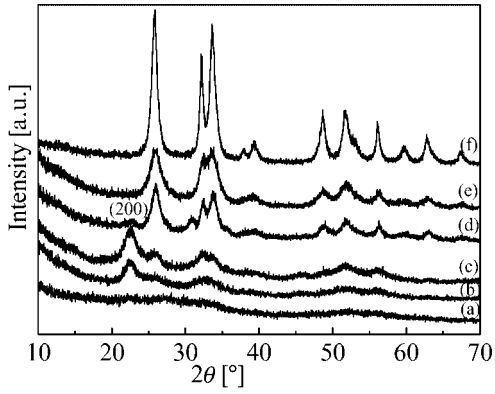

Figure 6. XRD patterns of the products obtained in the presence of ethylenediamine and at 210 °C with different heating time of (a) 1 h; (b) 2 h; (c) 6 h; (d) 8 h; (e) 12 h; and (f) 36 h.

$$In^{3+} + 3H_2O \rightarrow In(OH)_3 + 3H^+ \quad (1)$$

$$In(OH)_3 \rightarrow InOOH + H_2O \quad (2)$$

Additionally, it is found that the morphology and the phase of the products also depend on the solvents used in the synthesis process. A mixture of dimethyl formamide (DMF) and water as the solvent results in the growth of uniform InOOH nanowires rather than 3D structures. If dimethyl acetamide (DMA) is used as the solvent instead of DMF while all other conditions are kept unchanged, only aggregated InOOH nanorods are obtained (Figure 7a), which indicates that InOOH nanowires could not form in DMA medium. The experimental result reveals that DMF is favorable for the exhibition of the coordination template effect from En. Also, when varying the volume of deionized water, the formation of the products prepared is seriously affected. Figure 7b shows the TEM image of a sample obtained in the presence of 1 mL of deionized water; it indicates that the increase in water facilitates the formation of aggregated InOOH short nanorods. Moreover, if the amount of water is less than 0.25 mL or more than 5 mL, we cannot obtain pure InOOH, which denotes that the amount of water is a crucial factor in controlling the phase of the orthorhombic InOOH. This is possibly due to small amounts of water inhibiting the hydrolysis of In^{3+} and the abundant amount of water restraining dehydration of $In(OH)_3$ [Equations (1) and (2)]. These control experiments revealed that 3D InOOH architectures consisting of nanowires can be obtained when using a mixture of DMF (15 mL) and water with a volume between 0.25 and 0.4 mL.

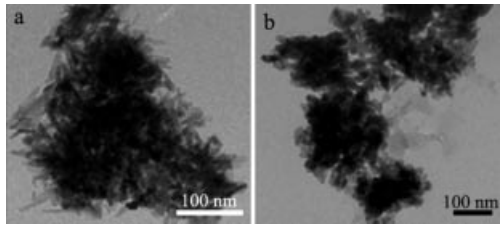

Figure 7. TEM images of samples: (a) when dimethyl acetamide was used as the solvent; (b) in the presence of deionized water (1 mL).

Combined with the above-mentioned discussion, a structure-directing coordination template mechanism under the ultrasonic-assisted conditions is proposed. The growth process of InOOH with hierarchical 3D architecture undergoes four distinctive stages: (1) Sonication induces the nucleation from the reaction of water, En, and In^{3+}. (2) Subsequently, many nanoparticles with small sizes are formed under the

solvothermal conditions and aggregate loosely due to the presence of the amido groups on the surface of the nanoparticles. Here, the phase of products formed in the stage is cubic $In(OH)_3$, which results from the hydrolysis of amorphous precursors. (3) Owing to the difference in solubilities of $In(OH)_3$ and InOOH, $In(OH)_3$ progressively dehydrolyzes to form InOOH. Simultaneously, InOOH nanorods are gradually obtained in the "dissolution–recrystallization" process of the particles of the precipitate as a result of the anisotropic crystal structure and the structure-directing coordination template effect from En, because En selectively adsorbs onto the lateral surfaces of the InOOH nanorods and restrains the lateral growth of the nanorods.[18] (4) With longer reaction times, all of the $In(OH)_3$ is eventually transformed into InOOH. Moreover, the nanorods would develop continuously into long nanowires and these nanowires could assemble into a 3D architecture because of the presence of hydrogen bonding between the hydroxy[5] and amido groups on the surface of the nanowires.

Finally, a UV/Vis spectrum was recorded with ethanol used as a reference to investigate the optical properties of the synthesized InOOH with a hierarchical 3D architecture. Figure 8 shows a typical UV/Vis spectrum; there is a broad absorption peak located at 279 nm (ca. 4.44 eV). Relative to the literature data of 3.5 eV,[11c] an obvious blueshift is observed, which can be attributed to the smaller diameters and larger aspect ratios of the nanowires.[19] The result from the UV/Vis spectrum indicates that InOOH is a wide band-gap semiconductor.

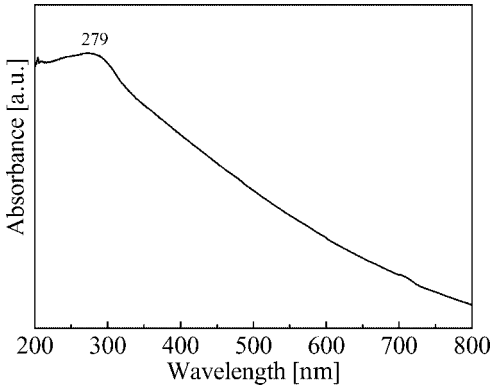

Figure 8. UV/Vis absorbance spectrum of InOOH with 3D architectures.

Conclusions

InOOH with a hierarchical 3D architecture was synthesized by a facile solvothermal route under the assistance of ultrasonic conditions. The phase and the morphology of the products were controlled by the choice of alkaline media and also the solvent. Sonication can help to form nucleation of uniform nanowires that assemble into 3D nanostructures. A possible structure-directing coordination template mechanism is proposed to explain the formation of InOOH with 3D hierarchical architectures. On the basis of a UV/Vis spectrum, InOOH is an important wide band-gap semiconductor. The present method is simple, and it can be extended to the preparation of other 3D nanostructured materials.

Experimental Section

Preparation of InOOH with a Hierarchical 3D Architecture: All reagents were of analytical grade, purchased from Shanghai Chemical Company, and used without further purification. In a typical procedure, $InCl_3{\cdot}4H_2O$ (0.5 mmol) and deionized water (0.25–0.40 mL) were mixed in a conical flask. After $InCl_3$ dissolution, dimethylformamide (15 mL) and ethylenediamine (5 mL) were added into the flask, and then the mixture was sonicated for about 1 h. The resulting solution was transferred to a 22-mL Teflon-lined autoclave, which was sealed and maintained between 210–220 °C for 24 h in a digital-temperature-controlled oven. The autoclave was cooled to room temperature naturally, and a white precipitate was collected by centrifugation and washed with distilled water and absolute ethanol several times, and dried in vacuo at 50 °C for 4 h.

Sample Characterization: The XRD patterns of the sample were recorded with a Philips X′pert X-ray diffractometer with Cu-k_α radiation (λ = 1.54187 Å). The morphology of the sample was observed with a JOEL JSM-6700 field emission scanning electron microscopy (FE-SEM). The nanostructures of the sample were analyzed with a JEOL-2010 transmission electron microscopy (TEM) at an acceleration voltage of 200 kV. The FTIR spectra were obtained with a PerkinElmer FTIR spectrometer. The ultraviolet and visible (UV/Vis) spectrum was recorded with a Shimadzu DUV-3700 spectrophotometer.

Acknowledgments

The financial support from the National Nature Science Research Foundation of China is gratefully acknowledged.

[1] a) C. N. R. Rao, A. K. Cheetham, *J. Mater. Chem.* **2001**, *11*, 2887–2894; b) C. N. R. Rao, A. MRller, A. K. Cheetham, *The Chemistry of Nanomaterials*, Wiley-VCH, Weinheim, **2004**; c) Y. N. Xia, P. D. Yang, Y. G. Sun, Y. Y. Wu, B. Mayers, B. Gates, Y. D. Yin, F. Kim, H. Q. Yan, *Adv. Mater.* **2003**, *15*, 353–389.
[2] Y. Cheng, Y. S. Wang, C. Jia, F. Bao, *J. Phys. Chem. B* **2006**, *110*, 24399–24402.
[3] X. X. Li, Y. J. Xiong, Z. Q. Li, Y. Xie, *Inorg. Chem.* **2006**, *45*, 3493–3495.
[4] L. S. Zhong, J. S. Hu, H. P. Liang, A. M. Cao, W. G. Song, L. J. Wan, *Adv. Mater.* **2006**, *18*, 2426–2431.
[5] J. Zhang, S. J. Liu, J. Lin, H. S. Song, J. J. Luo, E. M. Elssfah, E. Ammar, Y. Huang, X. X. Ding, J. M. Gao, S. R. Qi, C. C. Tang, *J. Phys. Chem. B* **2006**, *110*, 14249–14252.
[6] B. Liu, H. C. Zeng, *J. Am. Chem. Soc.* **2004**, *126*, 8124–8125.
[7] B. Liu, H. C. Zeng, *J. Am. Chem. Soc.* **2004**, *126*, 16744–16746.
[8] W. Q. Zhang, L. Q. Xu, K. B. Tang, F. Q. Li, Y. T. Qian, *Eur. J. Inorg. Chem.* **2005**, 653–656.
[9] Z. J. Gu, T. Y. Zhai, B. F. Gao, X. H. Sheng, Y. B. Wang, H. B. Fu, Y. Ma, J. N. Yao, *J. Phys. Chem. B* **2006**, *110*, 23829–23836.
[10] a) D. Routkevitch, T. Bigioni, M. Moskovits, J. M. Xu, *J. Phys. Chem.* **1996**, *100*, 14037–14047; b) H. Q. Cao, Z. Xu, H. Sang, D. Sheng, C. Y. Tie, *Adv. Mater.* **2001**, *13*, 121–123; c) M. H. Huang, S. Mao, H. Feich, H. Q. Yan, Y. Y. Wu, H. Kind, E. Weber, R. Russo, P. D. Yang, *Science* **2001**, *292*, 1897–1899; d) C. Z. Wu, Y. Xie, D. Wang, J. Yang, T. W. Li, *J. Phys. Chem. B* **2003**, *107*, 13583–13587; e) D. H. Wang, H. M. Luo, R. Kou,

M. P. Gil, S. G. Xiao, V. O. Golub, Z. Z. Yang, C. J. Brinker, Y. F. Lu, *Angew. Chem. Int. Ed.* **2004**, *43*, 6169–6173.
[11] a) W. S. Seo, H. H. Jo, K. Lee, J. T. Park, *Adv. Mater.* **2003**, *15*, 795–797; b) C. H. Lee, M. Kim, T. Kim, A. Kim, J. Paek, J. W. Lee, S. Y. Choi, K. Kim, J. B. Park, K. Lee, *J. Am. Chem. Soc.* **2006**, *128*, 9326–9327; c) H. L. Zhu, K. H. Yao, H. Zhang, D. R. Yang, *J. Phys. Chem. B* **2005**, *109*, 20676–20679.
[12] R. Roy, M. W. Shafer, *J. Phys. Chem.* **1954**, *58*, 372–375.
[13] a) D. B. Yu, S. H. Yu, S. Y. Zhang, J. Zuo, D. B. Wang, Y. T. Qian, *Adv. Funct. Mater.* **2003**, *13*, 497–501; b) C. L. Chen, D. R. Chen, X. L. Jiao, C. Q. Wang, *Chem. Commun.* **2006**, *44*, 4632–4634; c) M. Epifani, P. Siciliano, A. Gurlo, N. Barsan, U. Weimar, *J. Am. Chem. Soc.* **2004**, *126*, 4078–4079.
[14] a) K. S. Suslick, *Science* **1990**, *247*, 1439–1445; b) B. Gates, B. Mayers, A. Grossman, Y. N. Xia, *Adv. Mater.* **2002**, *14*, 1749–1752; c) B. T. Mayers, K. Liu, D. Sunderland, Y. N. Xia, *Chem. Mater.* **2003**, *15*, 3852–3858.
[15] a) Y. D. Li, H. W. Liao, Y. Ding, Y. T. Qian, L. Yang, G. E. Zhou, *Chem. Mater.* **1998**, *10*, 2301–2303; b) Y. D. Li, H. W. Liao, Y. Ding, Y. Fan, Y. Zhang, Y. T. Qian, *Inorg. Chem.* **1999**, *38*, 1382–1387; c) Z. X. Deng, C. Wang, X. M. Sun, Y. D. Li, *Inorg. Chem.* **2002**, *41*, 869–873; d) F. Gao, Q. Y. Lu, S. H. Xie, D. Y. Zhao, *Adv. Mater.* **2002**, *14*, 1537–1540.
[16] S. Gorai, D. Ganguli, S. Chaudhuri, *Cryst. Growth Des.* **2005**, *5*, 875–877.
[17] V. C. Farmer, *The Infrared Spectra of Minerals* (Translated into Chinese by: C. G. Li, Z. Li, Y. P. Ying, S. S. Wang, X. L. Han, Y. Q. Li), Science Press, Beijing, **1982**, p. 119.
[18] D. Xu, Z. P. Liu, J. B. Liang, Y. T. Qian, *J. Phys. Chem. B* **2005**, *109*, 14344–14349.
[19] a) B. M. I. Van der Zande, L. Pagès, R. A. M. Hikmet, A. van Blaaderen, *J. Phys. Chem. B* **1999**, *103*, 5761–5767; b) Y. F. Liu, J. B. Cao, J. H. Zeng, C. Li, Y. T. Qian, S. Y. Zhang, *Eur. J. Inorg. Chem.* **2003**, 644–647.

Received: April 3, 2007
Published Online: July 31, 2007

